Int J Thermophys (2009) 30:306–315
DOI 10.1007/s10765-008-0451-8

A CFD Study on a Calibration System for Contact Temperature Probes

F. Arpino · V. Fernicola · A. Frattolillo · L. Rosso

Published online: 6 June 2008

Abstract Surface-temperature measurements by means of contact probes require a detailed investigation of the probe-surface interaction. For an accurate calibration of such probes, the heat transfer processes involved in contact measurements must be well known and the impact of any influence parameters must be taken into account. At present, contact probes are generally calibrated by means of a temperature-controlled hot plate. A calibration system for contact surface-temperature probes, based on such a hot plate, was developed at INRIM. It covers the temperature range from ambient to 350 °C. The reference temperature is available on the upper surface of a metal block and is determined by linear extrapolation of the readings of three calibrated thermometers embedded into the block at different depths. However, the actual temperature of the reference surface largely depends on the sensor-to-surface interaction. The contact thermal resistance, the thermal conductivity of the block, the geometry of the probe, and the temperature of the surrounding fluid are just some of the parameters that affect a calibration and that may cause measurement errors if they are not properly taken into account and corrected for. Better insight into the interaction between the surface and the probe is therefore required. Since the experimental evaluation of measurement errors is not straightforward, mathematical modeling could represent a crucial tool to better understand the interactions between the probe and the calibration system. In this paper, a finite-element numerical model of the INRIM calibration system was developed in order to investigate the temperature field across the reference block as well as on its surface during a calibration. The thermal load introduced by a commercial

F. Arpino · A. Frattolillo
Department DIMSAT, University of Cassino, via Gaetano Di Biasio 43, 030343 Cassino, FR, Italy

V. Fernicola · L. Rosso (✉)
INRIM, Strada delle Cacce 73, 10135 Torino, Italy
e-mail: l.rosso@inrim.it
URL: http//www.inrim.it

contact probe during a calibration was also included in the simulation and its effect on the temperature field was studied. In order to obtain a detailed mathematical model, the surrounding air was also included in the simulation, avoiding the imposition of boundary conditions at the interface between solid parts and fluid. The proposed model was validated by comparing the results obtained with the available experimental data.

Keywords Calibration system · CFD · Contact probe · Surface thermometry

1 Introduction

Accurate contact measurements of surface temperature of solid bodies call for a detailed understanding of the interactions among the surface, the contact probe, and the surrounding environment, and knowledge of systematic measurement errors which stem from these interactions. In order to reduce such errors, operative procedures for field measurement and for the calibration must take into account various influence parameters, including the thermal coupling between surface and sensor (shape of the sensor, surface properties, contact thermal resistance, etc.) and the heat exchange with the surrounding medium (air temperature, air speed, etc.). According to the available literature, the deviation between the "true" surface temperature, i.e., the undisturbed temperature without the sensor, and the actual sensor output can be expressed as the sum of three contributions [1,2]: (i) error resulting from the change in the temperature field within the measurand, caused by the attached temperature sensor; (ii) error due to the contact resistance between the reference surface and the contact surface of the sensor; and (iii) error related to the intrinsic distance between the sensing element (a resistance or a metal junction) in the probe and the external surface of the probe itself. The experimental evaluation of these errors is not straightforward, as it depends both on the design of the contact sensor and on the measurand [3–5]. Besides, the uncertainty associated with the undisturbed temperature depends on the uncertainty of the measurement method; it is related to the pyrometer uncertainty in a direct radiometric measurement of surface temperature, while it is due to the uncertainty of the sensors embedded in the reference body when the surface-temperature extrapolation method is adopted [6]. In order to improve the sensor design to obtain better thermal contact with the surface, several simplified models have been proposed [7–10]. Nevertheless, a more systematic approach and a detailed model are desirable in order to better estimate the errors in temperature measurements during the calibration procedure.

A finite-element numerical procedure (FEM) [11] was recently proposed by the authors to determine the first and third systematic errors in contact temperature calibration systems and validated by simulating two calibration systems [12]. In this paper, such a numerical procedure was extended in order to investigate the influence of the heat transfer with the surrounding environment (air temperature, wall temperatures, and air speed) and a parametric analysis was performed. In particular, a steady-state two-dimensional axially symmetric mathematical model was proposed, which allows the calculation of temperature and velocity fields in the surrounding fluid, thus avoiding the approximations related to the estimation of convective heat transfer coefficient

between the solid parts and the surrounding fluid. The radiative heat transfer between the equipment surfaces and the surrounding environment was also taken into account. The latter was assumed to behave like a blackbody. The proposed model was validated by comparing the results obtained to the available experimental data obtained with a calibration system designed and constructed at INRIM.

Since the accuracy of the numerical results depends on the uncertainty of the thermal properties of the materials employed (such as the thermal conductivity of the reference block, the emissivity of the reference surface), a numerical investigation was carried out in order to evaluate the influence of these parameters. The thermal load introduced by a probe during a calibration was included in the simulation, and its effect on the temperature field was studied. Since the estimation of the thermal contact resistance is difficult (in fact, it depends on the contact cross section, the force and angle of attachment, the roughness and hardness of the surface, the air layers and impurities confined between the materials), the results are presented in terms of thermal perturbation of the reference surface.

2 Experimental Apparatus

The core of the calibration system for surface-temperature probes developed at INRIM is shown in Fig. 1. The reference temperature T_s is generated on the upper surface of a cylindrical aluminum alloy block (25 mm thick, 100 mm in diameter), the other surface being heated to the temperature $T(r, 25)$. The block is surrounded by thermal insulation and is provided with a coaxial active thermal guard in order to reduce radial heat loss, thus improving the uniformity of the surface temperature. In this configuration, a *quasi-linear* temperature gradient is obtained across the block. As a consequence, the surface temperature can be obtained through extrapolation of the temperatures measured by three calibrated Pt100 thermometers that are radially embedded in the block at different depths. The block temperature is controlled by an active control system with a separate Pt100-sensor, a PID controller, and a DC power supply.

3 Numerical Model and CFD Study

Accurate surface-temperature measurements require a detailed understanding of heat transfer processes occurring among the reference temperature surface, probe, and surroundings. In fact, the operation of a calibration system for contact surface-temperature

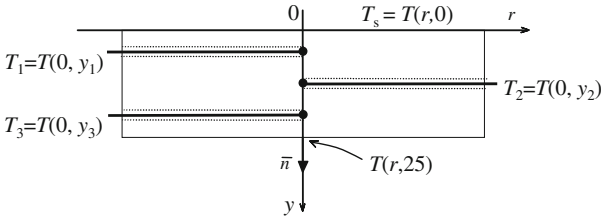

Fig. 1 Hot plate-based calibration system for contact temperature probes developed at INRIM

sensors involves a large number of parameters and different mechanisms of heat transfer that act simultaneously: heat conduction through solid bodies, convective heat transfer between the measurement surface and the surrounding fluid, as well as between the fluid and the sensor, and radiative heat transfer. Besides, the temperature field generates buoyancy forces, on which the velocity fields and the convective heat transfer coefficient depend. Since the experimental evaluation of errors affecting contact temperature measurements is not straightforward, computational fluid dynamic (CFD) techniques represent a very powerful tool for both design and optimization of contact surface-temperature sensor calibration systems. In particular, mathematical modeling techniques allow a detailed prediction of the temperature distribution over the calibration surface.

The numerical simulation was carried out for two cases, i.e., with and without the contact temperature probe applied on the reference surface. In order to accurately predict the temperature field in the aluminum cylindrical block, both solid and fluid domains have been modeled, thus avoiding the imposition of boundary conditions at the interfaces between the solid parts and the surrounding air. According to the geometrical features of the contact temperature sensor calibration system, a two-dimensional axially symmetric mathematical model was employed. In particular, the computational domain, together with the boundary conditions imposed and the computational grid employed, are sketched in Fig. 2, in the presence of the probe. The width of the domain was chosen in such a way to obtain an undisturbed flow field on the left side of the domain itself. With reference to Fig. 2, pressure, velocity, and temperature in the fluid domain have been predicted by the numerical solution of the following mass, momentum, and energy conservation equations:

$$\begin{aligned} &\nabla \cdot \mathbf{u} = 0 \\ &\mathbf{u} \cdot \nabla \mathbf{u} = -\nabla p + \nu_f \nabla^2 \mathbf{u} + \mathbf{g} \\ &\rho_f c_{pf} \mathbf{u} \cdot \nabla T = \nabla \cdot \left(k_f \nabla T \right) \end{aligned} \tag{1}$$

where $\mathbf{u}$ represents the velocity vector, p is the pressure, T is the temperature, ν_{f} is the fluid kinematic viscosity, ρ_{f} is the fluid density, $c_{p\mathrm{f}}$ is the fluid specific heat, and k_{f} represents the fluid thermal conductivity. The buoyancy term $\mathbf{g}$ in the momentum conservation equation, acting in the symmetry axis direction y (Fig. 2), has been calculated by imposing the Boussinesq approximation. In order to obtain a numerically tractable model for the fluid domain, the following assumptions have also been imposed: stationary conditions, the fluid was assumed to be incompressible, the flow field was assumed to be laminar, and the air was assumed to behave as an ideal gas. Equation 1 has been solved with appropriate boundary conditions. In particular, a "no slip" condition was assumed for the velocity field at the bottom side of the domain and at the interfaces between solid parts and fluid domain. In order to simulate an undisturbed field on the left side of the domain, a normal flow at ambient temperature was assumed to enter the domain from this side, while a free boundary condition was assumed at the top side of the domain. Finally, adiabatic conditions were imposed at the bottom and right sides of the computational domain.

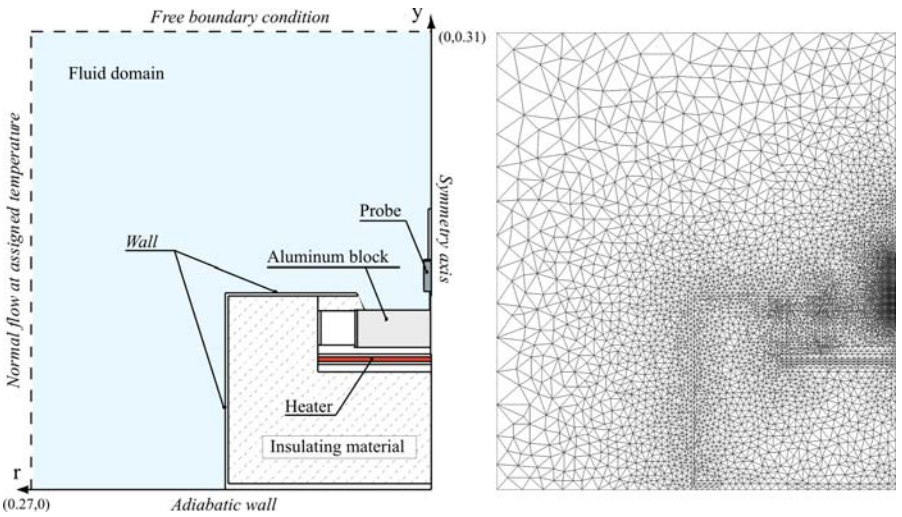

Fig. 2 Computational domain with boundary conditions (left) and computational grid employed in case of the presence of a dual-band contact probe, applied on the reference surface

The temperature field in the solid parts of the domain was simulated by solving the following heat equation:

$$\nabla \cdot (k_s \nabla T) + Q = 0 \tag{2}$$

where k_s represents the thermal conductivity of the solids and Q is a heat source/sink term. The thermal coupling between solid and fluid domains was guaranteed by imposing the temperature continuity condition at the interfaces between different domains. Finally, the radiative heat exchange between different solid surfaces and between solid surfaces and the surrounding fluid was taken into account by assuming that the latter behaves like a blackbody, while the solid surfaces were assumed to behave as a gray body with constant emissivity.

The above partial differential equations (PDEs) have been numerically solved by employing the Comsol® commercial code, based on finite elements. The computational domain was divided into sub-domains by using an unstructured computational grid, made of about 17,000 triangular elements. The number and the distribution of the elements composing the meshes were determined on the basis of an accurate grid sensitivity analysis. In particular, Fig. 2 shows the computational grid employed in the presence of the contact temperature probe, constituted by 17,149 triangular elements.

4 Results

The simulation allowed a detailed prediction of all the quantities of interest in both the solid and fluid domains and in the presence and absence of the contact temperature probe. Figure 3 shows the velocity contours (left) and the temperature field (right) when there is no probe on the temperature reference surface (top) and in the presence

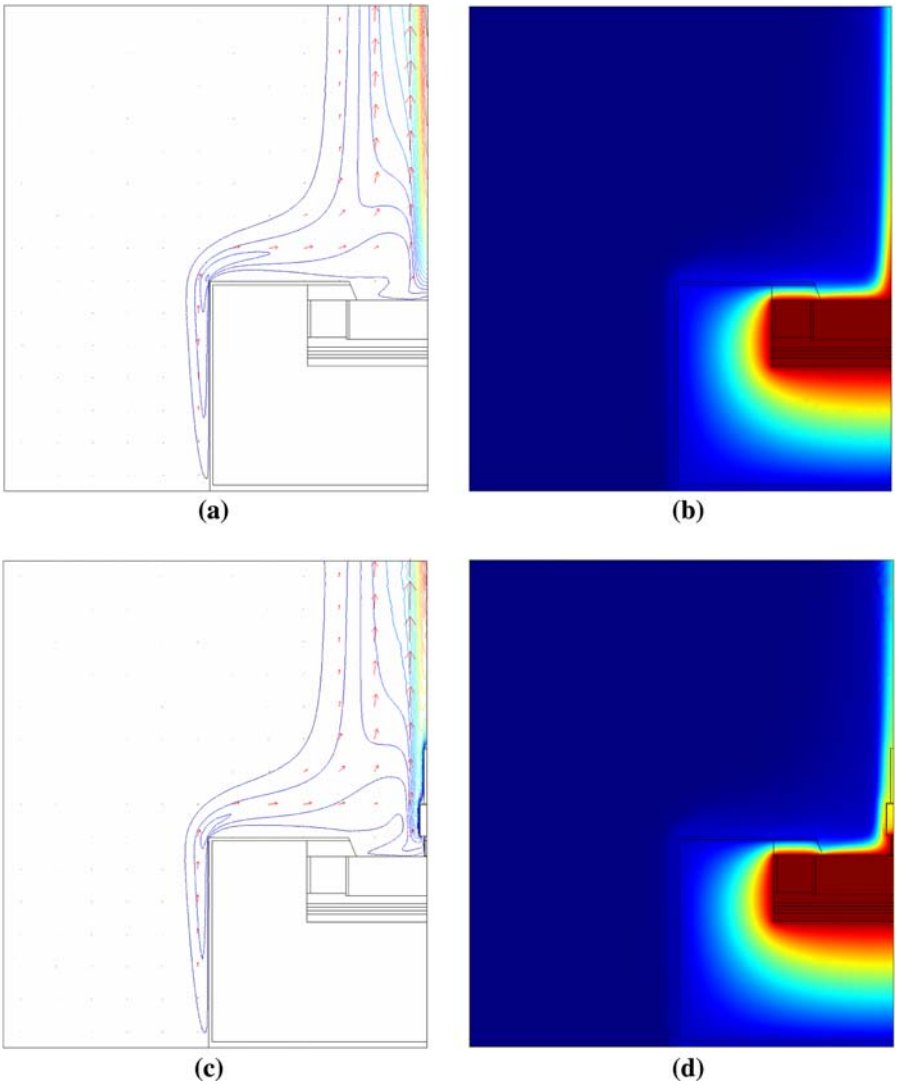

Fig. 3 Velocity contours (left) and temperature field (right) without (top) and with (bottom) a dual-band contact probe applied on the reference surface of the block, at 100 °C

of the probe (bottom). The fields reported in Fig. 3 have been calculated for a reference surface temperature of 100 °C. Interesting aspects of the numerical simulation can be derived from Fig. 3. The velocity and temperature fields show that the chosen domain width confirms the assumption of an undisturbed condition at the left side of the computational domain. Almost zero velocity and temperature gradient values were observed at the boundary. Also, from the analysis of Fig. 3, it is possible to notice the effect of the contact temperature probe on both the velocity and temperature fields. The maximum calculated air velocity was $0.627\,\mathrm{m}\cdot\mathrm{s}^{-1}$ in the absence of the probe, while

it slightly increased to $0.646\,\mathrm{m}\cdot\mathrm{s}^{-1}$ in the presence of the contact temperature probe. As a consequence, the presence of the probe is expected to increase the heat flux from the reference temperature surface to the surrounding environment. Even though such a difference is not qualitatively visible in Fig. 3, an accurate analysis of the temperature distribution across the block and over the reference surface is required.

4.1 Temperature Distribution Across the Block

The numerical and experimental results are reported in Figs. 4 and 5 for different surface temperatures. In particular, Fig. 4 shows the numerical temperature fields near the block reference surface, whose temperature was set at 300 °C, with and without a contact temperature probe applied to the surface. As expected, the presence of the probe slightly modifies the temperature field near the block reference surface. In the graphs presented, the coordinate origin was placed at point B and the directions of the r-axis and the y-axis were assumed as in Fig. 4, with point A at ($r = 50\,\mathrm{mm}$; $y = 0\,\mathrm{mm}$) and point C at ($r = 0\,\mathrm{mm}$; $y = 25\,\mathrm{mm}$). As a consequence, the position of the sensing element of the PRTs, which are radially embedded in the metal block at different depths, was described through the coordinates (0, 6.25), (0, 12.50), and (0, 18.75).

Figure 5 shows a comparison between the numerical temperature profile along the vertical axis of the block (BC axis) and the measurements of the embedded PRTs, at several surface temperatures, in the absence of the contact temperature probe (curve N). The linear tendency resulting from the numerical simulation is in good agreement with the experimental results (curve S). In fact, the average temperature difference was less than 0.04 °C over the whole temperature range. From the analysis of Fig. 5, it can also be seen that the disagreement slightly increases with the temperature, probably due to the assumption of constant thermal conductivity and emissivity of aluminum with temperature. In particular, the numerical temperature profiles show an increasing slope

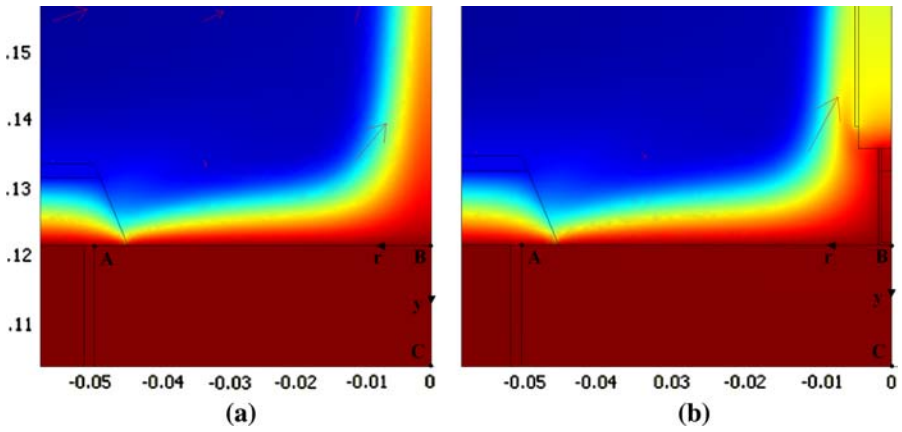

Fig. 4 Numerical temperature field near the reference surface of the block at 300 °C (**a**) without and (**b**) with a contact temperature probe applied on its surface

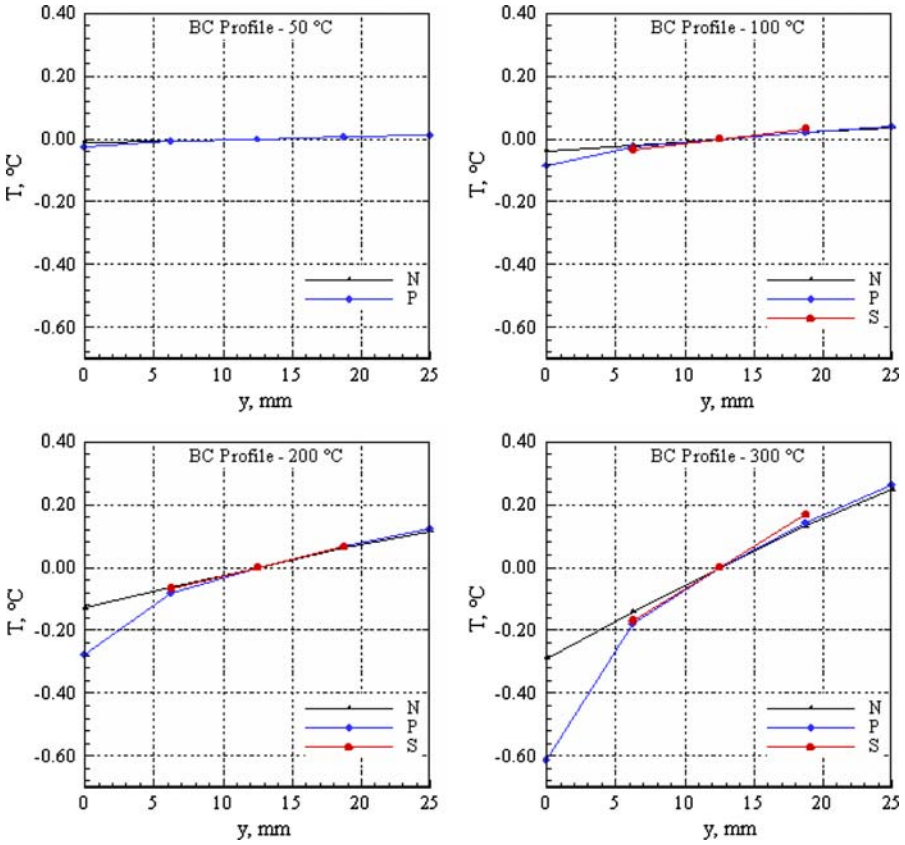

Fig. 5 Comparison between experimental (S curve) and calculated temperature profiles across the block (BC axis) with no probe on the surface (N curve) and when a probe is applied (P curve)

as the reference surface temperature increases. This is clearly due to the radiative heat flux, which increases with temperature.

When the application of a dual band-type contact probe on the reference surface was simulated, the perturbing effect generates the temperature profiles P depicted in Fig. 5, which clearly highlights how the presence of the probe causes a dramatic distortion of the temperature field, resulting in a nonlinear temperature gradient near the surface of the block. In particular, the temperature distortion from linearity ranges from 0.04 °C at 100 °C up to 0.3 °C at 300 °C.

4.2 Temperature Field on the Reference Surface

The model was also used for the numerical simulation of the temperature field on the upper surface of the block, and the results thus obtained were compared to the experimental data. Figure 6 depicts, for different reference surface temperatures, the temperature profile predicted by the model for two different thermal conditions, i.e.,

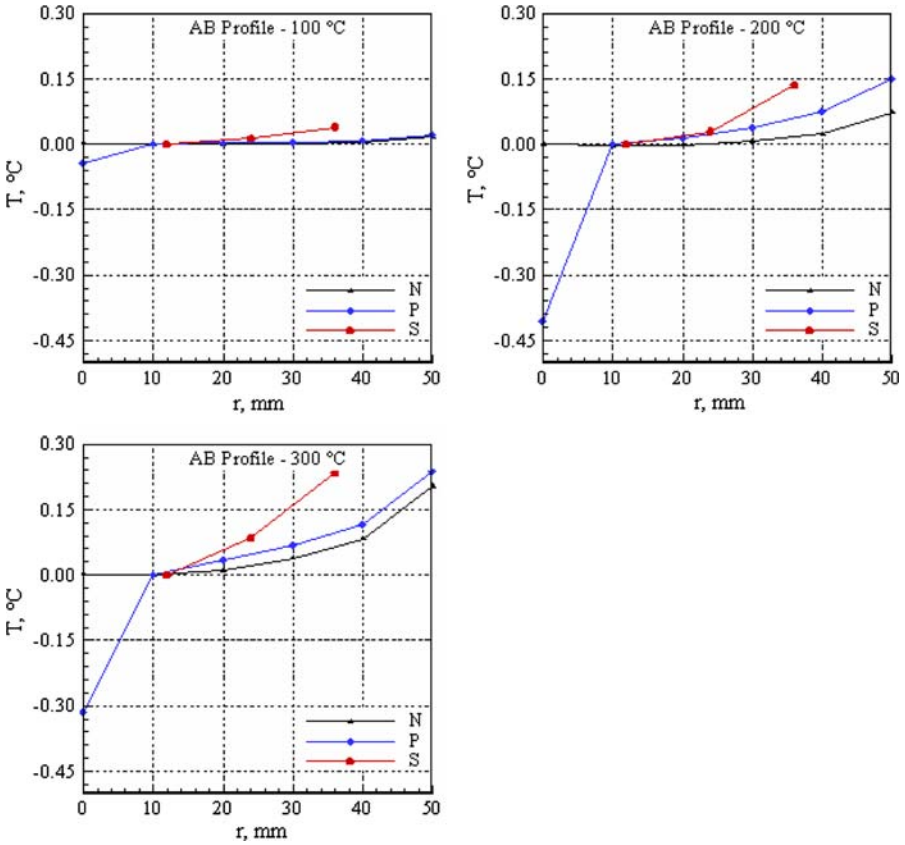

Fig. 6 Comparison between experimental (S curve) and calculated temperature profiles on the upper surface of the reference block with no probe on the surface (N curve) and when a probe is applied on its surface (P curve)

with and without the probe applied to the surface (curve P and curve N, respectively), as well as the experimental temperature profile (curve S) with the probe. The latter was obtained through measurements of the surface temperature at three radial positions using fluorescence decay-time thermometry [13]. The numerical results indicate that the surface uniformity deteriorates as the temperature increases. In the intermediate region, where the numerical and experimental results were compared, the agreement is always better than 0.15 °C. The numerical modeling also predicted a rapid decrease in temperature as it neared the probe position ($r = 0$).

The differences between the numerical and experimental results can be attributed to errors in the emissivity of the surface oxide layer, errors in the thermal conductivity of the metal block, as well as to the approximations used in modeling the probe.

5 Conclusions

A detailed CFD study of the probe-to-surface interaction in a calibration system for contact surface-temperature probes is presented. Such a calibration system, which

is based on a temperature-controlled hot plate, was developed at INRIM. It operates from ambient temperature to 350 °C. A steady-state two-dimensional axially symmetric mathematical model, which enables the prediction of the temperature field both in fluid and solid regions, was developed. The radiative heat transfer between the apparatus surfaces and the surrounding air was also taken into account. The tests carried out at several surface temperatures showed good agreement between the numerical and experimental results. The maximum difference in the temperature distribution across the reference block, with no probe applied, was within 0.04 °C, slightly increasing with temperature. When the probe was placed on the reference surface, the distortion of the temperature profile, near its application point, produced in the solid a nonlinear variation that increased with temperature.

As regards the surface-temperature distribution when the probe is applied, the model underestimated the actual profile. The proposed model can be further refined. In particular, the emissivity and the thermal conductivity of the material can be accurately measured in order to reduce the error due to their estimation.

References

1. L. Michalski, K. Eckersdorf, J. Mc Ghee, *Temperature Measurement*, 2nd edn. (John Wiley & Sons, New York, 2001)
2. M.J. Reader-Harris, C.D. Stewart, A.B. Forbes, G.J. Lord, Continuous Modelling in Metrology, *National Physical Laboratory Report* (Teddington, UK, 2000)
3. D.K. Hennecke, E.M. Sparrow, Int. J. Heat Mass Tran. **13**, 287 (1970)
4. E.M. Sparrow, in *Measurement in Heat Transfer*, 2nd edn., ed. by E.R.G. Eckert, R.J. Goldstein (McGraw-Hill Inc., Washington, 1976)
5. B. Cassagne, G. Kirsch, J.P. Bardon, Int. J. Heat Mass Tran. **23**, 1207 (1980)
6. F. Edler, M. Gorgieva, J. Hartmann, M. Wagner, in *Proceedings of TEMPMEKO 2001, 8th International Symposium on Temperature and Thermal Measurements in Industry and Science*, ed. by B. Fellmuth, J. Seidel, G. Scholz (VDE Verlag, Berlin, 2002), pp. 1105–1110
7. N.R. Keltner, J.V. Beck, ASME Trans.—J. Heat Tran. **105**, 312 (1983)
8. F. Bernhard, S. Augustin, H. Mammen, K.D. Sommer, E. Tegeler, M. Wagner, U. Demisch, P. Trageser, in *Proceedings of TEMPMEKO '99, 7th International Symposium on Temperature and Thermal Measurements in Industry and Science*, ed. by J.F. Dubbeldam, M.J. de Groot (Edauw Johannissen bv, Delft, 1999), pp. 257–262
9. L. Michalski, K. Eckersdorf, J. McGhee, in *Proceedings of Workshop on "Surface thermal measurements"* (Budapest, Hungary, 1995)
10. D. Zvizdic, Measurement **16**, 247 (1995)
11. O.C. Zienkiewicz, R. L. Taylor, *The Finite Element Method*, 5th edn. (Butterworth and Heinemann, London, 2000)
12. F. Arpino, A. Frattolillo, N. Massarotti, in *Proceedings of ICCES World Congress 2004* (Madeira, Portugal, 2004)
13. L. Rosso, V.C. Fernicola, A. Tiziani, in *Temperature, Its Measurement and Control in Science and Industry*, vol. 7, part 2, ed. by D.C. Ripple (AIP, Melville, New York, 2003), pp. 1045–1050